PHYSICAL REVIEW D VOLUME 36, NUMBER 11 1 DECEMBER 1987

Spin splittings of heavy-quark bound states from lattice QCD

Massimo Campostrini
Istituto Nazionale di Fisica Nucleare, Sezione di Pisa, Pisa, Italy
and Brookhaven National Laboratory, Upton, New York 11973

Kevin Moriarty
Institute for Advanced Study, Princeton, New Jersey 08540
and John Von Newman National Supercomputer Center, 665 College Road East, Princeton, New Jersey 08543

Claudio Rebbi
Physics Department, Boston University, Boston, Massachusetts 02215
and Physics Department, Brookhaven National Laboratory, Upton, New York 11973
(Received 15 May 1987)

The spin-dependent potentials which determine the spin splittings of heavy-quark bound states are evaluated by a lattice Monte Carlo calculation. One of the spin-orbit potentials is found to have a long-range nonperturbative component, while all other potentials exhibit a short-ranged perturbative behavior. Calculations at two different values of the bare coupling constant demonstrate scaling. The spin splittings that follow from the calculated potentials are evaluated. Good agreement is found with experimental data provided that vacuum-polarization effects from $q\bar{q}$ pairs at short distances are taken into account.

I. INTRODUCTION

One of the most important tests for any theory of particle interactions is its capability of predicting the correct spectrum of bound-state masses. The calculation of mass levels in quantum chromodynamics (QCD) involves the long-range behavior of the interaction between quarks. Such a behavior cannot be determined by the standard analytical tool, namely, a perturbative expansion; however, as has become dramatically apparent during the last few years, it is one of the nonperturbative features of the theory which can be reliably inferred from lattice numerical calculations.

Two strategies can be followed for a numerical calculation of the spectrum. One can evaluate the Green's functions for the products of operators creating and annihilating composite states with definite quantum numbers. The masses are then determined from the rate of decay of the Green's functions as the Euclidean time separation increases. This method involves no restriction on the relativistic features of the quark motion, but can produce reliable results for the lowest masses of the states with given quantum numbers at best. Alternatively, assuming that the masses of the constituent quarks are large and that their motion is essentially nonrelativistic, one can describe the bound states in the framework of a Schrödinger equation. The numerical calculations are then used to determine the potential functions which enter into the Schrödinger equation.

Fundamental to this second approach, which is the one we shall be concerned with in this paper, is an expansion of the equation for the bound states of two heavy quarks into powers in the inverse quark mass.[1,2] The ensuing Hamiltonian to leading order contains a single scalar potential $V(r)$. $V(r)$, which is the QCD potential between static sources with the color quantum numbers of quark and antiquark, is one of the observables best determined by lattice numerical calculations.[3-7] At the next order, one encounters the potentials $V_1 - V_4$ which determine the spin-orbit and spin-spin interactions between quarks. The behavior of the spin potentials at small separations can be determined from perturbation theory, but earlier assumptions that such potentials only had a short-range component were found to be inconsistent.[8] One then faces again the nonperturbative problem of determining the long-range properties of the interaction.

The evaluation of the spin potentials $V_1 - V_4$ is also amenable to lattice numerical calculations. It is, however, a much more demanding calculation than the one required to compute the scalar potential V. If one wishes to obtain phenomenologically relevant results one must perform the calculation on a lattice of rather large extent and with high statistics. In this paper we wish to report the results of one such calculation. Given the complexity of the calculation, we developed a code aimed at taking full advantage of the vectorized capabilities of a modern supercomputer.[9] The code was then applied to a calculation of the spin-dependent potentials on a $16^3 \times 32$ lattice at two different values of the SU(3) coupling parameter: namely, $\beta(\equiv 6/g^2) = 6$ and $\beta = 6.2$. As we shall see, the accuracy we achieve is sufficient to produce reliable information on the long-range behavior of the potentials and, indeed, to evaluate the spin splittings from first principles, with no intervening adjustable parameter.

Our calculation has been performed within the so-called quenched approximation to QCD, by which vacuum-polarization effects associated to the creation and annihilation of quark-antiquark pairs are left out. In Ref. 10 it was found, however, that the modification of the scalar potential at short distances from such po-

larization effects is crucial for the possibility of reproducing the spectrum of spin-averaged excitations of the heavy-quark families. We shall find a similar situation insofar as the spin splittings are concerned. One can argue that the required modifications, being at short distances, are under control of perturbation theory and can be determined. Indeed, if we correct the quenched results along the lines of Ref. 10, the ensuing spin splittings turn out in good agreement with experimental data.

Some of our results for the spin-dependent potentials have been presented in Ref. 11. This paper expands our previous communication with the results at a different value of β, which permits a verification of scaling, and with the explicit application to the evaluation of the spin splittings. Earlier numerical results for the spin-dependent potentials have been published in Refs. 12–15. The investigations of Refs. 12–15 dealt with different gauge groups or could achieve more limited statistics, so that no direct comparison with our results is possible. However, Ref. 15 reaches for the pattern of long-range behavior the same conclusions, which we infer from our analysis. The plan of the paper is as follows. In Sec. II we review the form of the spin-dependent terms in the Hamiltonian and the relation between the spin-dependent potentials and lattice observables. In Sec. III we present the results of our Monte Carlo numerical calculation. In Sec. IV the lattice results are applied to the calculation of the spin splittings for the states of the J/ψ and Υ families. The role of the vacuum-polarization effects is also discussed there. Finally, Sec. V presents a few words in conclusion.

II. THE SPIN-DEPENDENT POTENTIALS

The propagator for a quark-antiquark pair simplifies under the assumption that the quarks are very massive. It is indeed then possible to describe their motion by a two-body Hamiltonian, whose terms are ordered in a series expansion into inverse powers of the quark mass.[1,2] To order $1/m^2$ this Hamiltonian takes the form

$$H=\frac{\mathbf{p}^2}{m}+V(r)+\frac{\mathbf{S}_+\cdot\mathbf{L}_++\mathbf{S}_-\cdot\mathbf{L}_-}{2m^2}\frac{1}{r}\left[\frac{dV}{dr}+2\frac{dV_1}{dr}\right]+\frac{\mathbf{S}_+\cdot\mathbf{L}_-+\mathbf{S}_-\cdot\mathbf{L}_+}{m^2}\frac{1}{r}\frac{dV_2}{dr}$$
$$+\frac{1}{m^2}[(\mathbf{S}_+\cdot\hat{\mathbf{r}})(\mathbf{S}_-\cdot\hat{\mathbf{r}})-\tfrac{1}{3}\mathbf{S}_+\cdot\mathbf{S}_-]V_3(r)+\frac{1}{3m^2}\mathbf{S}_+\cdot\mathbf{S}_-V_4(r)\ . \tag{2.1}$$

The static potential $V(r)$ and the spin-dependent potentials $V_i(r)$ are universal, the only dependence on the flavor of the quarks coming through their mass. [It must be noticed, however, that the derivation of Eq. (2.1) involves taking the limits of large mass and large time interval of propagation in a certain order, and that it has been argued in the literature that nonuniversal terms, containing logarithms of mass ratios, should also be included.[16]] The potentials in Eq. (2.1) can be related to the expectation values of transport factors for the color gauge field with or without suitable insertions of chromoelectric fields. Precisely, given a set of gauge-covariant observables $O(x)$, such as the chromomagnetic or chromoelectric fields, $B_i(x)$ and $E_i(x)$, respectively, for any closed path γ going through the points x_1, x_2, . . . , we define

$$\langle O(x_1)O(x_2)\cdots\rangle_W=\left\langle \mathrm{Tr}P\left[\exp\left[ig\oint_\gamma A_\mu(x)dx^\mu\right]O(x_1)O(x_2)\cdots\right]\right\rangle\ , \tag{2.2}$$

$\langle\ \rangle$ representing the ordinary quantum-mechanical expectation value in Euclidean space-time.

According to this definition $\langle O(x_1)O(x_2)\cdots\rangle$ is the quantum-mechanical expectation value of the path-ordered product of the observables and transport factors for the path γ. In particular, $\langle 1\rangle_W$ is the expectation value of the transport factor itself, or Wilson loop factor. In the following we shall consider only rectangular paths with a spacelike basis vector $\mathbf{r}$ corresponding to the separation between the quark and the antiquark, and the height in the temporal direction, corresponding to an interval of propagation T of the $q\bar{q}$ pair.

The potentials $V(r)$ and $V_i(r)$ are then given by the equations[1,2]

$$V(r)=-\lim_{T\to\infty}\frac{\ln\langle 1\rangle_W}{T}\ ,$$
$$\epsilon_{ijk}\hat{\mathbf{r}}_k\frac{d\tilde{V}_1(r,T)}{dr}=\int_0^T dt\int_0^T dt'(t'-t)\langle g^2B_i(0,t)E_j(0,t')\rangle_W\ ,$$
$$\epsilon_{ijk}\hat{\mathbf{r}}_k\frac{d\tilde{V}_2(r,T)}{dr}=\int_0^T dt\int_0^T dt'(t'-t)\langle g^2B_i(0,t)E_j(\mathbf{r},t')\rangle_W\ , \tag{2.3}$$
$$(\hat{\mathbf{r}}_i\hat{\mathbf{r}}_j-\tfrac{1}{3}\delta_{ij})\tilde{V}_3(r,T)+\tfrac{1}{3}\delta_{ij}\tilde{V}_4(r,T)=\int_0^T dt\int_0^T dt'\langle g^2B_i(0,t)B_j(\mathbf{r},t')\rangle_W\ ,$$
$$V_i(r)=\lim_{T\to\infty}\frac{1}{T}\frac{\tilde{V}_i(r,T)}{\langle 1\rangle_W}\ .$$

The short-distance behavior of all the potentials can be determined analytically, through perturbative considerations, but any long-distance component must be of nonperturbative origin. The potentials can however be determined numerically, throughout the range of phenomenologically relevant separations, by a Monte Carlo calculation of the quantum averages appearing in Eq. (2.3). The numerical results at short distances can only

serve to check the validity of the calculational technique, but, at large distances, they provide genuine new information.

The numerical calculation proceeds through the formulation of QCD on a lattice. The dynamical variables are color-SU(3) matrices defined over the oriented links of a hypercubical lattice, with lattice spacing a. The quantum-mechanical expectation values are given by

$$\langle O \rangle = Z^{-1} \int \prod_{x,\mu} dU_x^\mu O(U) \exp[-S_G(U)] ,$$
$$Z = \int \prod_{x,\mu} dU_x^\mu \exp[-S_G(U)] , \tag{2.4}$$

where S_G is the gauge action, for which we assume Wilson's form:

$$S_G(U) = \beta \sum_{x,\mu \le \nu} \tfrac{1}{3} \mathrm{Re\,Tr}(1 - U_x^{\mu,\nu}) ,$$
$$U_x^{\mu\nu} = U_x^{\nu\dagger} U_{x+\hat{\nu}a}^{\mu\dagger} U_{x+\hat{\mu}a}^{\nu} U_x^{\mu} . \tag{2.5}$$

β in Eq. (2.5) is the coupling parameter, related by $\beta = 6/g^2$ to the bare coupling constant g. The continuum limit is achieved by letting a and g approach 0 simultaneously, according to a well-defined renormalization relation.

The transport factors in Eq. (2.2) are given, over the lattice, by products of the gauge dynamical variables U_x^μ. The chromoelectric and chromomagnetic fields can be rendered by different lattice expressions, which, while all equivalent in the continuum limit, can produce different results at small lattice separations. In our calculation we have transcribed E_i and B_i over the lattice as follows. We denote by $U_{x,ss'}^{\mu\nu}$ $(s,s' = \pm 1)$ the product of the link variables U_x^μ along a closed square path, originating at x, with further vertices in $x + s\hat{\mu}a$, $x + s\hat{\mu}a + s'\hat{\nu}a$, and $x + s'\hat{\nu}a$, and oriented counterclockwise in the plane. For example,

$$U_{x,-+}^{\mu\nu} = U_{x-\hat{\mu}\alpha}^{\mu} U_{x-\hat{\mu}\alpha}^{\nu\dagger} U_{x-\hat{\mu}\alpha+\hat{\nu}\alpha}^{\mu\dagger} U_x^{\nu} . \tag{2.6}$$

In terms of these variables we define lattice-field strengths

$$F_{x,ss'}^{\mu\nu} = \mathrm{Im} U_{x,ss'}^{\mu\nu} \equiv -\tfrac{1}{2} i (U_{x,ss'}^{\mu\nu} - U_{x,ss'}^{\mu\nu\dagger}) , \tag{2.7}$$

$$F_{x,s}^{\mu\nu} = \tfrac{1}{2} \sum_{s'} F_{x,ss'}^{\mu\nu} , \tag{2.8}$$

$$F_x^{\mu\nu} = \tfrac{1}{2} \sum_{s} F_{x,s}^{\mu\nu} . \tag{2.9}$$

In order to evaluate the correlations between **B** and **E** fields and the correlations between the components of **B** in the direction of separation r, we made the identifications

$$ga^2 B_i(x) \Longrightarrow F_x^{jk} , \quad ijk \text{ in cyclical order} ,$$
$$ga^2 E_i(x) \Longrightarrow F_x^{4i} . \tag{2.10}$$

We used, however,

$$\tfrac{1}{2} \sum_{s} \langle F_{x,s}^{ij} F_{x',s}^{ij} \rangle \tag{2.11}$$

to reproduce the correlation between components B_k orthogonal to the direction of separation (assumed to be along the i axis). The motivation for this last definition is in the fact that the components of **B** orthogonal to **r** are defined over spacelike plaquettes with one side in the **r** direction. At short distances the correlations are quite sensitive to the separation between the centers of the plaquettes in the **r** direction and, by the prescription of Eq. (2.11), we include in the averaging only plaquettes with the correct r separation. The definitions of Eqs. (2.10) and (2.11) were tested in Ref. 12, in connection to a study of the spin-dependent potentials for the lattice formulation of QED, and found to produce good agreement with perturbative results even at small separations.

III. THE MONTE CARLO CALCULATION

We formulated the theory on a $16^3 \times 32$ lattice with periodic boundary conditions, the long axis being identified with the time axis, and performed two simulations at the values $\beta = 6$ and $\beta = 6.2$ of the coupling parameter. Each simulation consisted of 6000 iterations from a cold start, by the Metropolis algorithm, with 10 hits per link and an acceptance of approximatively 50%. 2000 iterations were used for equilibrium and the observables were then measured every 20 iterations for the balance of the simulations. We thus collected measurements over 200 lattice configurations at each value of β, including, in the averages, the factors corresponding to all loops in the lattice with a spacelike basis ranging from 0 to $7a$, and the other side in the temporal direction, with extent $4a \le T \le 12a$.

We used the variance-reduction technique of Ref. 17 for the calculation of the transport factors associated with the bases of the loops. Namely, the values of the U_x^μ variables entering into the basis factors were replaced by their averages over 100 hits of the Metropolis algorithm, performed while keeping all the neighboring variables fixed. To maintain the required statistical independence, we summed over the chromomagnetic-field insertions, in the integrals of Eq. (2.3), only for $a \le t$, $t' \le T - a$. All chromoelectric insertions can be included, because the r components of the electric fields never appear in the expression for the potentials. We associated to the chromoelectric fields temporal coordinates equal to those of the centers of the timelike plaquettes over which they are defined [an alternative definition of $E(x,t)$ would make the use of averages of plaquette variables consecutive in the temporal direction].

We performed the entire computation on the Cyber 205 computer at the Eastern Cybernet Center in Rockville, Maryland. It is a 2 pipe, 8 Megaword machine, over which our code runs, mostly in 32 bit arithmetic, at an average speed slightly higher than 100 Mflops. The calculation is, however, very demanding and, in spite of the impressive computational resources, would not have been feasible if we had not taken advantage of the freedom of performing gauge transformations and of some additional time-saving procedures, in order to simplify the computation. We have presented the details of our code in a separate publication.[9] Let us only mention here briefly its most relevant features.

Computationally, the main simplification comes from performing the calculation of the loop factors in the temporal gauge. This eliminates the need of evaluating the transport factors, of varying length, associated with the temporal sides of the loops, and gives the additional advantage that the insertions corresponding to the chromoelectric and chromomagnetic fields can be accumulated while they are computed, so that the loops need to be closed once only for the whole integral. More specifically, in a first step of the code for the measurement of the observables, the gauge configuration is transformed to the temporal gauge $U_x{}^4=1$. The periodicity in time is not maintained after the gauge transformation, and therefore we extended the lattice in time by the amount necessary to contain all measurable loops. In a second step, the code calculates averages of the transport factors associated with the bases of the loops, so as to implement the variance-reduction technique mentioned above. In the process, the field strengths are also calculated (the corresponding plaquette variables must be evaluated anyway for the Metropolis procedure), and field strengths and basis transport factors are temporarily stored in large memory. Finally, in a double loop over the time coordinate and time extent of the loops, the appropriate combinations of the field strengths are summed and combined with the basis transport factors so as to reproduce the required integrals.

The results of our numerical simulation are reproduced in Tables I and II and in Figs. 1–4. The tables give the measured values for the Wilson loop factors and for the integrals of the loop factors with insertions $\tilde{V}_i$ [cf. Eq. (2.3)]. They also reproduce the parameters of the linear fits to the time dependence of the ratios $\tilde{V}_i/(T\langle 1\rangle_W)$. The coefficients of the linear terms give the spin-dependent potentials in lattice units [cf. Eq. (2.3)]. The tables give the results of fits to the dependence on time to the whole range of measured values $4a-12a$. We have also done fits in the range $5a-12a$ and evaluated the potentials from the differences of the values of the above ratios at successive values of T, finding consistent results. We estimated the errors by repeating the calculation of all dynamical variables over subsamples of measurements, obtained by leaving out sets of approximatively 20 consecutive measurements. The errors are then evaluated from the variance of the results from the subsamples, following a procedure very similar to the one adopted in Ref. 18. These are the errors quoted in the tables. We also calculated the errors from the quadratic fluctuations of the individual measurements, finding generally consistent results. The discrepancies ($\lesssim 30\%$) between the two different determinations of the errors can be explained by the overestimate or underestimate of various correlations in the second procedure.

Our results show very clearly that the potential V_1 has a long-range component, consistent with a constant behavior of $dV_1(r)/dr$ for larger r. V_2-V_4, instead, all appear to decrease rather rapidly with increasing r, exhibiting short-range behavior only. In particular, V_4, which is $\propto\delta^3(r)$ to lowest order in perturbation theory, differs from 0 only in the immediate neighborhood of the origin.

For small r, one would expect the spin-dependent potentials to agree with the predictions from perturbation theory. This gives, to leading order,

$$V_1=0\ ,\quad V_2=-\frac{4}{3}\frac{\alpha_s}{r}\ ,\quad V_3=4\frac{\alpha_s}{r^3}\ ,$$
$$V_4=2\nabla^2V_2=-\frac{32\pi}{3}\alpha_s\delta^3(r)\ ,\quad \alpha_s=g_s{}^2/4\pi\ , \tag{3.1}$$

g_s being the renormalized QCD coupling constant. On the other hand, one also expects the lattice results to be affected by the discreteness of the lattice when r equals only a few lattice spacings. To estimate the magnitude of errors induced by the lattice for small separations, we calculated correction factors based on the following idea. The correlations among the field strengths in Eq. (2.3) are given by averages which involve several plaquettes. The central points of these plaquettes are not all at separation r; rather they are at separations r' which may substantially differ from r at a small lattice distance. The correction factors are then obtained by rescaling the contributions of the plaquettes by the factors [either $(r/r')^2$ or $(r/r')^3$] which would follow from first-order perturbation theory. In Figs. 2–4 we plot the potentials before [symbols $\square$ ($\beta=6$) and $\triangle$ ($\beta=6.2$)] and after [symbols $\circ$ ($\beta=6$) and $\times$ ($\beta=6.2$)] multiplication by the correction factors. Our correction factors are not meant to account for the lattice artifacts in any rigorous way, but only to give an indication of the likely magnitude of lattice distortions. We see that while these are rather pronounced for $r=a$, they become almost negligible at $r=2a$ already. We will comment on the fits in Figs. 1–4 in the next section.

The representation of $V_i(r)$ in physical units, as in Figs. 1–4, involves multiplication by suitable renormalization factors. We converted the dimensionless lattice results into physical units by multiplying, first, potentials and separations by the appropriate power of $a(\beta)$, for which we assumed the asymptotic scaling formula

$$a=\frac{1}{\Lambda}\left[\frac{8\pi^2\beta}{33}\right]^{51/121}\exp\left[-\frac{4\pi^2\beta}{33}\right] \tag{3.2}$$

with lattice scale parameter $\Lambda=4.14$ MeV. This value for Λ is taken from the calculation of the string tension in quenched QCD of Refs. 3 and 4, which was done on a lattice having the same extent as the present one and with comparable statistics. Indeed, our results for the Wilson loop factors are consistent with those of Ref. 3.

An additional renormalization factor f is required to convert the bare, lattice values of the spin-dependent potentials to renormalized ones. In Ref. 11 we determined such a factor on the basis of the following, heuristic consideration. The spin-dependent potentials always appear in the Hamiltonian divided by m^2, m being the quark mass. Since the energy levels must be a renormalization-group invariant, it is plausible that the lattice values for the potentials should be divided by the bare, Lagrangian mass squared m_0. Equivalently, they should

TABLE I. Results of the Monte Carlo calculation at $\beta=6$. All quantities are in units of 10^6 times the appropriate power of a. The table contains the values of the Wilson loop factors W, of the Wilson loop factors with insertions (loop values) $d\tilde{V}_1/dr$, $d\tilde{V}_2/dr$, $\tilde{V}_3$, $\tilde{V}_4$, integrated over t and t' but not divided by W, and of the coefficients of the linear term in the linear fits from $t=4a$ and to $12a$ to the ratios between loop values and Wilson loop factors. For computational reasons, the weights in the fits are based on the errors from the quadratic fluctuations, rather than those in the table. This does not introduce any significant bias, since the two determinations of the errors produce compatible results.

$T \backslash r$	0	1	2	3	4	5	6	7
				Wilson loop factors				
4	1 000 000	167 087	55 002	22 534	9 946	4 500	2 054	936
	±0	±52	±64	±37	±24	±13	±9	±8
5	1 000 000	110 670	30 124	11 048	4 486	1 888	806	336
	±0	±46	±40	±33	±21	±10	±9	±8
6	1 000 000	73 326	16 529	5 448	2 040	783	326	128
	±0	±42	±34	±22	±21	±8	±5	±6
7	1 000 000	48 580	9 070	2 685	950	329	139	44
	±0	±34	±32	±23	±14	±5	±7	±6
8	1 000 000	32 178	5 009	1 331	428	157	61	13
	±0	±35	±31	±22	±9	±11	±8	±4
9	1 000 000	21 316	2 752	663	181	60	25	7
	±0	±33	±21	±17	±10	±7	±5	±5
10	1 000 000	14 127	1 510	344	72	18	4	0
	±0	±33	±23	±20	±9	±8	±6	±5
11	1 000 000	9 373	824	183	29	8	−6	−2
	±0	±36	±19	±11	±10	±4	±5	±4
12	1 000 000	6 201	445	105	35	6	−5	−7
	±0	±32	±22	±12	±14	±9	±5	±3
				Spin potential V_1: loop values				
4	0	−4 134	−1 422	−553	−245	−109	−49	−19
	±0	±11	±6	±7	±4	±3	±2	±2
5	0	−3 997	−1 136	−399	−167	−63	−23	−7
	±0	±16	±13	±12	±6	±5	±4	±2
6	0	−3 468	−826	−275	−104	−27	−21	−16
	±0	±15	±14	±13	±8	±11	±5	±5
7	0	−2 851	−556	−171	−50	−30	−15	−3
	±0	±28	±27	±23	±9	±12	±9	±8
8	0	−2 269	−349	−95	−33	−32	−31	17
	±0	±39	±21	±25	±23	±19	±9	±7
9	0	−1 703	−219	19	−3	−10	−17	16
	±0	±67	±34	±28	±21	±15	±14	±11
10	0	−1 243	−122	−4	−26	3	5	−20
	±0	±84	±56	±42	±18	±19	±18	±11
11	0	−825	−94	−22	10	−42	−30	24
	±0	±96	±50	±66	±37	±20	±26	±18
12	0	−538	−37	−50	32	−49	−58	6
	±0	±132	±59	±43	±51	±39	±24	±16
				Spin potential V_2: loop values				
4	0	39 964	3 098	346	51	9	−2	−1
	±0	±23	±23	±8	±7	±7	±3	±4
5	0	37 056	2 577	268	24	0	−1	−4
	±0	±45	±25	±13	±9	±11	±7	±4
6	0	31 648	1 929	185	2	11	6	−3
	±0	±69	±31	±25	±18	±12	±9	±6
7	0	25 694	1 357	88	8	19	10	−7
	±0	±78	±45	±29	±22	±21	±14	±15
8	0	20 134	826	37	12	27	21	−7
	±0	±104	±37	±36	±18	±36	±13	±17
9	0	15 428	530	24	−17	43	1	−7
	±0	±120	±63	±54	±37	±30	±24	±16

TABLE I. (*Continued*).

T \ r	0	1	2	3	4	5	6	7
				Spin potential V_2: loop values				
10	0	11 572	333	−4	−4	46	36	4
	±0	±142	±89	±82	±46	±38	±29	±20
11	0	8 490	206	22	35	15	−18	1
	±0	±163	±130	±104	±47	±52	±36	±35
12	0	6 077	175	62	140	−9	−6	1
	±0	±166	±153	±122	±36	±55	±48	±33
				Spin potential V_3: loop values				
4	−438 462	25 504	2 283	306	50	14	2	−1
	±25	±20	±19	±5	±5	±4	±4	±3
5	−593 523	23 318	1 813	242	30	11	2	6
	±46	±25	±20	±10	±5	±6	±5	±5
6	−748 616	19 715	1 303	174	20	−7	−3	6
	±71	±30	±21	±13	±12	±7	±4	±6
7	−903 710	15 904	898	117	16	4	21	4
	±97	±37	±27	±11	±12	±8	±5	±5
8	−1 058 795	12 440	587	85	32	15	24	7
	±123	±44	±22	±14	±9	±12	±9	±8
9	−1 213 872	9 475	391	57	43	10	19	4
	±153	±47	±31	±20	±12	±11	±10	±8
10	−1 368 954	7 099	266	50	34	−17	11	−10
	±185	±38	±34	±29	±19	±16	±12	±10
11	−1 524 038	5 256	180	3	14	−10	−5	−1
	±218	±37	±33	±25	±23	±7	±14	±10
12	−1 679 113	3 808	117	−2	−1	−8	−14	3
	±252	±52	±35	±26	±25	±16	±10	±13
				Spin potential V_4: loop values				
4	2 017 901	−16 196	−1116	−88	−6	6	8	2
	±199	±43	±27	±12	±10	±7	±7	±3
5	2 734 875	−13 479	−761	−66	−7	6	17	−4
	±287	±52	±34	±22	±7	±16	±8	±6
6	3 452 136	−10 714	−463	−36	8	−3	22	−8
	±373	±61	±36	±22	±11	±17	±12	±8
7	4 169 426	−8 292	−311	−28	28	−32	5	−5
	±461	±74	±45	±25	±19	±17	±10	±7
8	4 886 726	−6 320	−215	−23	42	−11	−28	3
	±556	±80	±37	±38	±25	±21	±13	±17
9	5 603 994	−4 742	−165	30	2	8	4	4
	±668	±71	±26	±37	±36	±14	±18	±11
10	6 321 246	−3 546	−169	−6	0	5	44	2
	±783	±58	±41	±52	±30	±17	±24	±12
11	7 038 517	−2 649	−176	−30	7	−7	11	−10
	±902	±69	±54	±44	±34	±33	±20	±11
12	7 755 736	−1 982	−170	3	25	−34	5	−39
	±1006	±77	±66	±30	±31	±28	±15	±15
				Spin potential V_1 from linear fit				
4	0	−11 304	−11 879	−12 041	−12 471	−9 272	−10 335	−10 937
	±0	±76	±352	±944	±882	±2 702	±4 650	±4 779
5	0	−11 145	−11 856	−13 146	−11 286	−11 086	−46 177	−78 760
	±0	±290	±473	±2 510	±3 669	±10 168	±10 822	±37 439
				Spin potential V_2 from linear fit				
4	0	96 099	29 680	8 597	−207	1 853	4 379	−11 235
	±0	±364	±672	±1 398	±2 761	±3 373	±8 346	±10 776
5	0	96 874	30 713	6 810	−1 564	21 846	27 727	−30 139
	±0	±773	±1 893	±4 228	±8 132	±19 180	±27 183	±59 842

TABLE I. (*Continued*).

T \ r	0	1	2	3	4	5	6	7
				Spin potential V_3 from linear fit				
4	−155 082	58 199	18 843	9 156	2 866	481	5 786	20 717
	±27	±195	±428	±923	±1 216	±3 774	±5 926	±13 981
5	−155 086	58 381	19 302	11 196	8 199	−5 083	33 832	31 537
	±28	±321	±865	±1 878	±4 223	±8 100	±12 936	±26 051
				Spin potential V_4 from linear fit				
4	717 222	−24 832	−4 807	−1 818	2 010	−3 257	18 279	−19 713
	±100	±362	±885	±1 641	±1 678	±6 981	±10 504	±16 584
5	717 274	−24 956	−5 118	−1 147	11 829	−21 890	14 790	−36 474
	±105	±537	±1 436	±3 924	±5 477	±16 699	±29 572	±49 167

be rescaled by a factor $f=(m/m_0)^2$, to be used in the Schrödinger equation in conjunction with a renormalized quark mass m. A calculation of hadronic masses in the quenched approximation, done on a lattice equal in size to the present one and with $\beta=6$ (Ref. 19), suggests $m/m_0\simeq 2$, for quarks giving origin to mesons comparable in mass to the lowest excitations of the J/ψ family. This gives then a value ≈ 4 for f, which is the one we used to express V_1-V_4 in physical units in Ref. 11.

Here we would like however to use a slightly different determination of the renormalization factor f. On the basis of Lorentz invariance, Gromes[8] has derived a relation among the potentials in Eq. (2.1): namely,

$$V+V_1-V_2=0\ . \tag{3.3}$$

The pattern of long-range behavior, namely, $dV_1/dr\to$const, $dV_2/dr\to 0$, which emerges from the lattice calculation, is consistent with such relation. Even more remarkable is that, as observed in Ref. 11, by rescaling V_1 according to the factor inferred from the calculation of masses, the magnitude of dV_1/dr is also brought in rather good agreement with Gromes's relation. Therefore, it appears to us that a better determination of the rescaling factor can be obtained by assuming the validity of Gromes's relation for asymptotic separations. A fit of dV_1/dr to the string tension, $\sigma=420$ MeV, gives then $f=4.6$, which is the factor we finally used to obtain the physical values of V_1-V_4. We notice that such value for f is consistent, giving the various sources of error, with the value formerly derived from the calculation of masses. The prescription based on Eq. (3.3) is, however, computationally more precise.

The verification of scaling, in the comparison of the data at $\beta=6$ and at $\beta=6.2$, is not affected by the value assumed for f (f can change only through an anomalous dimension factor, whose variation between the two values of β is negligible). From Figs. 1–4 we see that scaling is rather well satisfied. The most relevant verification of scaling comes from V_1, which, contrary to V_2-V_4, is not dominated by a scale-invariant perturba-

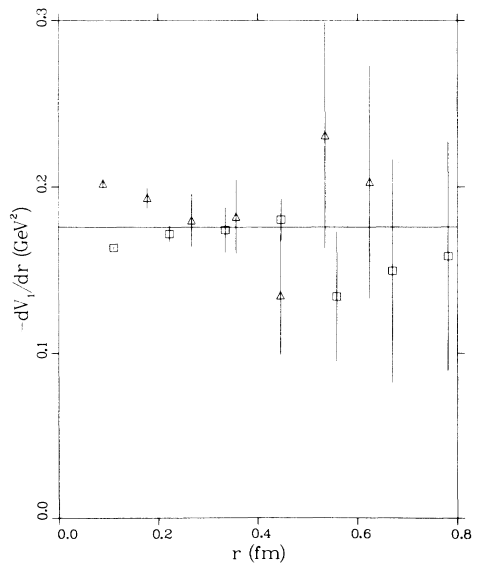

FIG. 1. Values for the spin potential dV_1/dr, in physical units, after the renormalization discussed in the text. The squares and triangles represent the results obtained at $\beta=6$ and 6.2, respectively.

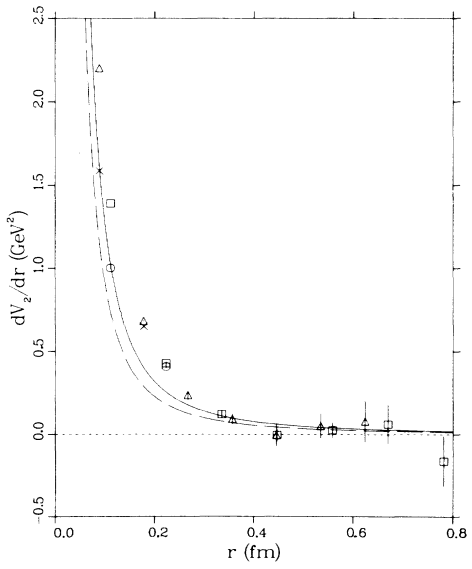

FIG. 2. Same as in Fig. 1, but for the spin potential dV_2/dr. The additional symbols represent the results at $\beta=6$ (circles) and $\beta=6.2$ (crosses), after a correction for lattice artifacts at small distances. The lines represent the lowest-order perturbative behavior with $\alpha_s=0.244$ (solid line) and $\alpha_s=0.175$ (broken line).

TABLE II. Same as in Table I, but for $\beta=6.2$.

T \ r	0	1	2	3	4	5	6	7
				Wilson loop factors				
4	1 000 000	191 276	71 574	32 989	16 305	8 261	4 210	2 162
	±0	±68	±66	±75	±47	±35	±24	±13
5	1 000 000	131 110	41 812	17 720	8 258	3 987	1 935	949
	±0	±61	±56	±50	±33	±25	±17	±9
6	1 000 000	89 902	24 484	9 552	4 216	1 954	908	430
	±0	±59	±44	±36	±24	±18	±12	±8
7	1 000 000	61 663	14 355	5 170	2 155	957	436	197
	±0	±56	±39	±30	±20	±17	±12	±9
8	1 000 000	42 290	8 431	2 811	1 117	483	206	92
	±00	±52	±33	±23	±17	±13	±8	±6
9	1 000 000	29 009	4 949	1 535	577	259	102	42
	±0	±53	±29	±14	±7	±8	±7	±4
10	1 000 000	19 896	2 897	836	311	126	43	20
	±0	±56	±23	±16	±10	±8	±7	±5
11	1 000 000	13 639	1 692	443	159	69	11	12
	±0	±52	±29	±12	±13	±10	±9	±6
12	1 000 000	9 356	1 010	242	80	46	7	12
	±0	±43	±30	±14	±16	±8	±8	±7
				Spin potential V_1: loop values				
4	0	−3 849	−1 420	−596	−284	−131	−65	−33
	±0	±10	±6	±4	±3	±3	±2	±2
5	0	−3 802	−1 182	−460	−209	−87	−49	−23
	±0	±13	±14	±9	±9	±6	±6	±3
6	0	−3 399	−913	−330	−149	−55	−32	−15
	±0	±26	±16	±16	±10	±10	±7	±4
7	0	−2 879	−652	−221	−85	−35	−24	−1
	±0	±38	±30	±30	±17	±11	±13	±7
8	0	−2 401	−430	−116	−34	−15	−22	−10
	±0	±56	±42	±40	±21	±12	±11	±9
9	0	−1 925	−307	−69	−30	−7	1	−6
	±0	±57	±43	±44	±38	±25	±20	±14
10	0	−1 537	−210	−21	12	10	−15	14
	±0	±53	±60	±32	±46	±43	±19	±14
11	0	−1 166	−164	26	75	5	20	−20
	±0	±93	±58	±53	±35	±27	±23	±13
12	0	−742	−85	29	−26	50	24	−11
	±0	±102	±57	±72	±31	±48	±23	±31
				Spin potential V_2: loop values				
4	0	45 811	3 974	489	68	11	−4	−1
	±0	±23	±10	±8	±6	±3	±5	±3
5	0	44 036	3 547	446	55	0	5	9
	±0	±30	±12	±11	±12	±11	±7	±5
6	0	38 985	2 851	340	55	8	−1	−7
	±0	±44	±20	±20	±18	±17	±12	±8
7	0	32 801	2 149	252	62	21	−5	−7
	±0	±55	±13	±41	±34	±22	±11	±10
8	0	26 643	1 551	141	84	−14	6	−21
	±0	±66	±47	±47	±36	±34	±20	±14
9	0	21 058	992	140	63	−28	11	0
	±0	±78	±52	±53	±32	±38	±18	±19
10	0	16 318	613	157	54	14	48	−59
	±0	±100	±89	±52	±34	±38	±44	±19
11	0	12 479	432	55	79	−10	−11	21
	±0	±121	±156	±82	±74	±35	±36	±17
12	0	9 464	264	141	177	−51	−30	11
	±0	±172	±173	±104	±79	±47	±48	±30

TABLE II. (*Continued*).

$T \backslash r$	0	1	2	3	4	5	6	7
				Spin potential V_3: loop values				
4	−431 242	30 112	3 078	455	82	14	4	0
	±20	±10	±13	±10	±8	±4	±3	±3
5	−584 224	28 476	2 594	373	71	19	9	2
	±32	±15	±16	±9	±10	±6	±4	±4
6	−737 246	24 927	1 948	273	62	6	2	0
	±44	±23	±15	±14	±13	±9	±9	±3
7	−890 275	20 814	1 387	181	79	10	7	−4
	±60	±26	±18	±14	±16	±10	±7	±5
8	−1 043 310	16 821	945	111	73	23	17	−2
	±75	±35	±22	±15	±13	±9	±10	±6
9	−1 196 354	13 268	654	52	61	5	7	−1
	±91	±51	±39	±26	±14	±6	±10	±10
10	−1 349 391	10 307	445	−17	43	9	−11	−5
	±107	±66	±45	±22	±23	±13	±11	±10
11	−1 502 422	7 908	315	−20	40	13	−9	4
	±124	±77	±43	±31	±19	±22	±8	±14
12	−1 655 458	5 980	217	−9	61	0	24	−16
	±141	±74	±40	±35	±19	±24	±12	±12
				Spin potential V_4: loop values				
4	1 964 378	−20 676	−1 757	−196	−10	1	−12	1
	±209	±28	±22	±16	±14	±5	±7	±6
5	2 664 774	−17 927	−1 298	−138	−6	−6	−5	9
	±315	±36	±24	±25	±13	±10	±6	±5
6	3 365 516	−14 823	−830	−74	0	−17	−2	−3
	±415	±52	±26	±32	±20	±9	±12	±8
7	4 066 305	−11 918	−498	−17	−35	−7	−5	−2
	±519	±66	±24	±33	±12	±15	±13	±9
8	4 767 109	−9 382	−264	19	−85	−2	−6	−13
	±611	±75	±35	±38	±21	±18	±12	±10
9	5 467 867	−7 324	−193	60	−63	−3	−4	0
	±715	±88	±52	±25	±26	±18	±18	±13
10	6 168 608	−5 654	−168	69	−47	−20	33	−12
	±832	±94	±63	±38	±17	±26	±18	±19
11	6 869 344	−4 350	−137	81	−22	−6	56	−40
	±948	±96	±79	±56	±30	±22	±26	±18
12	7 570 094	−3 313	−183	63	−54	−3	18	−19
	±1 064	93	76	69	18	26	20	20
				Spin potential V_1 from linear fit				
4	0	−8 899	−8 521	−7 928	−8 026	−5 941	−10 168	−8 942
	±0	±125	±286	±710	±979	±1 591	±2 990	±3 087
5	0	−8 977	−8 632	−7 762	−7 651	−5 821	−12 281	−6 981
	±0	±287	±708	±2 061	±3 077	±5 297	±8 564	±9 446
				Spin potential V_2 from linear fit				
4	0	96 943	30 056	10 511	4 212	−191	2 341	3 559
	±0	±138	±207	±939	±1 424	±3 155	±3 407	±5 617
5	0	97 807	31 784	11 117	10 615	4 091	−2 019	−28 079
	±0	±336	±749	±2 485	±4 341	±7 971	±10 990	±17 691
				Spin potential V_3 from linear fit				
4	−153 022	59 959	18 395	7 044	5 814	2 664	3 369	77
	±15	±169	±273	±513	±1 285	±1 561	±3 347	±2 168
5	−153 033	60 156	17 368	6 335	12 746	2 718	4 077	−5 862
	16	332	712	1 061	3 269	3 395	7 159	9 584
				Spin potential V_4 from linear fit				
4	700 702	−28 578	−4 698	−347	−2 088	−2 689	193	2 117
	±106	±342	±546	±1 512	±1 611	1 651	4 178	6 918
5	700 767	−28 650	−2 107	3 275	−8 680	−5 133	−1 045	−19 806
	±108	±616	±1 030	±3 008	±3 492	±4 840	11 886	18 361

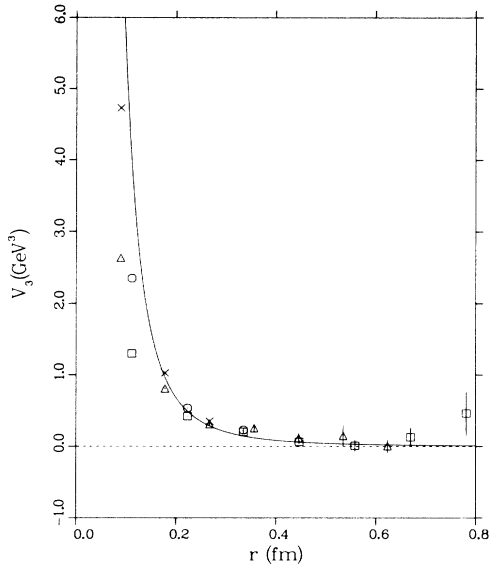

FIG. 3. Same as in Fig. 2, but for the spin potential V_3. The line represents the lowest-order perturbative behavior with $\alpha_s = 0.175$.

tive contribution. The scaling of V_1 in physical units implies a substantial variation of its lattice values from $\beta = 6$ to $\beta = 6.2$ and, with the exception of the lowest lattice separation where lattice artifacts may be particularly important, appears very well satisfied.

IV. APPLICATION TO HEAVY-QUARK SPECTROSCOPY

The numerical results, obtained for a few discrete values of the separation between quarks, must be interpolated by a smooth function in order to be used for the actual calculation of energy levels. The limited accuracy

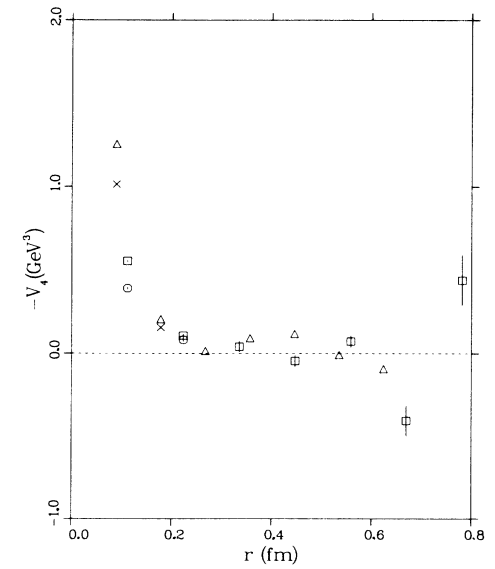

FIG. 4. Same as in Figs. 2 and 3, but for the spin potential V_4.

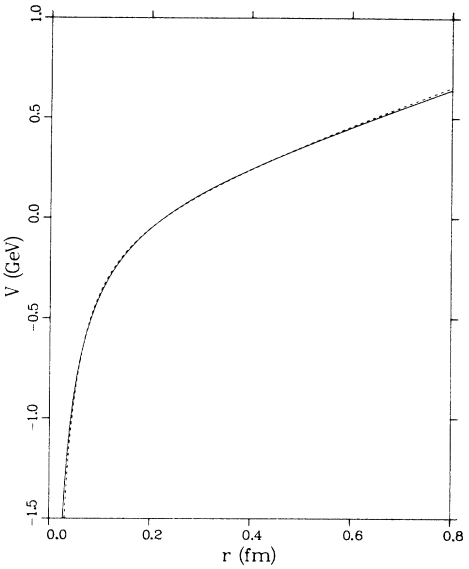

FIG. 5. The static potential V_0, as determined from the results of Refs. 3 and 4, and its best fit in terms of a linear plus Coulomb potential, using the square of the $1P$ $b\bar{b}$ wave function as weight for the fit.

of the numerical results does not warrant fits with several free parameters and the observed pattern of short- and long-range behavior suggests then that dV_1/dr (cf. Fig. 1) be fit by a constant function and all other potentials by the lowest-order perturbative expressions of Eq. (3.1).

As a consequence of our renormalization procedure, the constant in the fit of dV_1/dr is the string tension itself. Gromes's relation would also imply that the strong coupling constant α_s in the fit of dV_2/dr is the same one

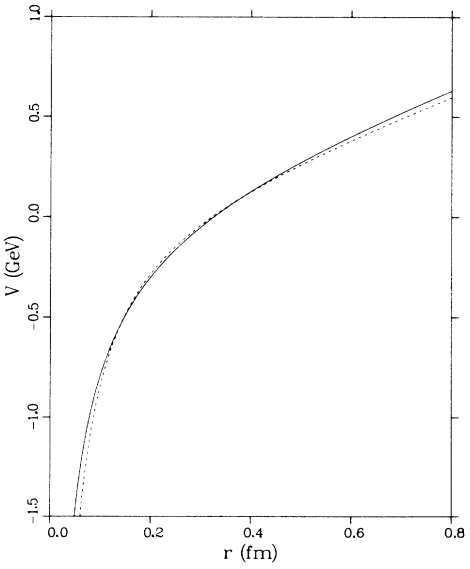

FIG. 6. Same as in Fig. 5, but for the static potential modified by the short-distance screening effects from three flavors of light quarks (cf. Ref. 10).

TABLE III. Values obtained for the spin-splittings in correspondence to different parameters used in the representation of the potentials V_1-V_4. In columns 1, 3, and 6, all short-distance behaviors are parametrized in terms of common strong coupling constant α_s. In columns 2 and 4, a different α_s [α_{2s}] is used to parametrize V_2 [and V_4, cf. Eq. (3.1)]. All splittings are in MeV. r is the ratio of the splittings of the $3P$ states.

	$\alpha_s=0.175$	$\alpha_s=0.175$ $\alpha_{2s}=0.244$	$\alpha_s=0.351$	$\alpha_s=0.351$ $\alpha_{2s}=0.489$	Experiment	$V_1'=-\sigma/2$
J/ψ						
$1(1S1)$-$1(1S0)$	49.1	68.4	98.3	136.9	115.9 (2.0)	98.3
$1(3P2)$-$1(3P1)$	−0.9	10.3	22.0	44.5	45.6 (0.6)	45.9
$1(3P1)$-$1(3P0)$	16.7	22.4	45.5	56.7	95.8 (1.2)	57.3
$r(1P)$	−0.054	0.460	0.485	0.785	0.476 (0.010)	0.801
$1(1P1)$-$1(3P1)$	−2.4	3.2	7.2	18.4		19.1
$2(1S1)$-$2(1S0)$	33.6	46.9	67.2	93.8	92.0 (5.0)	67.2
Υ						
$1(1S1)$-$1(1S0)$	35.3	49.1	70.5	98.2		70.5
$1(3P2)$-$1(3P1)$	7.1	12.7	18.4	29.6	21.4 (0.9)	22.7
$1(3P1)$-$1(3P0)$	12.0	14.8	26.3	31.9	32.1 (1.5)	28.5
$r(1P)$	0.592	0.858	0.700	0.928	0.667 (0.049)	0.779
$1(1P1)$-$1(3P1)$	2.6	5.4	7.3	12.9		9.4
$1(3D3)$-$1(3D2)$	−0.1	1.9	4.3	8.2		8.7
$1(3D2)$-$1(3D1)$	1.5	2.8	6.0	8.8		9.1
$1(1D2)$-$1(3D2)$	−0.3	0.3	0.8	2.1		2.2
$2(1S1)$-$2(1S0)$	18.6	25.9	37.1	51.8		37.1
$2(3P2)$-$2(3P1)$	6.1	10.6	15.3	24.4	12.9 (1.1)	18.5
$2(3P1)$-$2(3P0)$	10.0	12.2	22.4	26.1	25.2 (2.4)	23.1
$r(2P)$	0.610	0.869	0.683	0.935	0.512 (0.073)	0.801
$2(1P1)$-$2(3P1)$	2.3	4.6	6.1	10.6		7.8
$3(1S1)$-$3(1S0)$	14.7	20.5	29.4	41.0		29.4

that would appear in a Coulomb plus linear fit to the scalar potential V. Figure 5 illustrates the result of such a fit. The solid line represents there the scalar potential, as derived in Refs. 3 and 4, whereas the dashed line gives the fit

$$V(r)=-\frac{4}{3}\frac{\alpha_s}{r}+\sigma r+\text{const} \quad \text{with } \alpha_s=0.175 \ , \quad (4.1)$$

which is obtained by minimizing the square deviation, weighted by the square of the wave function of the $1P\Upsilon$ states. If we insert the value thus derived for α_s in the perturbative formulas of Eq. (3.1), we obtain for V_2 and V_3 the values represented by the dashed-dotted curve in Fig. 2 and by the solid curve in Fig. 3. The resulting fit to V_3, considering also that the first two points at one unit of lattice separation are most likely affected by lattice distortions, can be deemed satisfactory. The dashed-dotted curve in Fig. 2 appears, however, to underestimate the numerical values. A fit to the points at all separations (and corrected for lattice artifacts as discussed in Sec. III) produces the value $\alpha_s=0.244$ and the solid curve in Fig. 2. (The points at an intermediate separation remain slightly above the fit. This could be seen as an indication of additional contributions beyond the lowest-order perturbative formula, but, at the present stage of accuracy of the numerical results, we do not feel that pursing such an interpretation would be warranted.)

The expression obtained for the spin-dependent potentials from the fits discussed above can be used to calculate the spin-splittings in the J/ψ and Υ families. The results of the calculation, based on first-order perturbation theory for the spin-dependent terms in the Hamiltonian and on the unperturbed wave functions obtained from the scalar potential after correction for quark vacuum-polarization effects,[10] are reproduced in Table III. The first column gives the splittings calculated assuming a common value, $\alpha_s=0.175$, in all short-range potentials V_2-V_4. The second column uses the higher value $\alpha_{2s}=0.244$ for V_2 [and V_4, according to Eq. (3.1)], determined from the fit to the Monte Carlo data. (We do not reproduce in the table the errors that would follow from the statistical errors in the Monte Carlo calculation because they would be underestimates of the real margins of error determined by various systematic effects, which are less quantifiable but which our discussion makes, we believe, apparent.)

The experimental results are reproduced in the fifth column. We see that, irrespective of the choice for the coupling constant in V_2, the theoretical values are too small to account for the experimentally observed spin

splittings and, also, that the pattern of splittings is in qualitative disagreement with experiment, as evidenced by the ratios $r=(m_{^3p_2}-m_{^3p_1})/(m_{^3p_1}-m_{^3p_0})$. However, we recall that the calculation has been performed in the quenched approximation and that quark vacuum-polarization effects can modify substantially the inter-quark potential at small separations. Indeed it has been found in Ref. 10 that the quenched results for the scalar potential V produce splittings among spin-averaged masses which are approximatively 30% smaller than the observed ones. At short distances it is, however, possible to correct for quark vacuum-polarization effects in a perturbative manner, and then one finds excellent agreement between the computed spin-averaged masses and the experimental ones.

In order to perform a similar correction also to the spin-dependent potentials, we proceeded as follows. We performed the same linear plus Coulomb fit, as discussed above, to the scalar potential after correction for quark vacuum-polarization effects. The result, illustrated in Fig. 6, gives a strong coupling constant $\alpha_s=0.351$. We see that the net effect of the quark polarization effects on the scalar potential at short distances is to rescale, by a factor very close to 2, the effective strong coupling constant (this agrees with the notion that the quarks screen the color charge: screening implies a reduction of the running coupling constant at large distances and an increase at short distances). Consistently with Gromes's relation, we assume that a similar rescaling should apply to the short-distance component of the spin-dependent potentials as well. The splittings calculated with the rescaled values are reproduced in the third and fourth columns of Table III. We see that the theoretical values are now in much better agreement with the experimentally observed ones, especially those in the third column which correspond to a common value for the coupling constant in the Coulombic part of all potentials. The spin splittings of the $1P$ level of the J/ψ family only turn out too small in comparison with the experimental results, although the experimental and theoretical values for the r ratios are in agreement. This discrepancy is not peculiar to the present analysis, and could be due either to relativistic effects or to the fact that the corresponding wave function extends to a domain where critical cancellations between the contributions of V_1 and V_2 take place, enhancing the consequences of any error in the determination of the potentials.

The last column in Table III gives the splittings obtained by reducing V_1 by a factor of 2. Since V, V_1, and V_2 enter in the determination of the splittings in the combination $\frac{1}{2}V+V_1+V_2$, taking $dV_1/dr=-\frac{1}{2}\sigma$ is tantamount to assuming the absence of any long-range component in the interaction determining the splittings. We see that, as has been noticed earlier in the literature, this worsens the agreement between theoretical and experimental values for the ratios of the P-wave splittings. Since in first-order perturbation theory the splittings are linear functions of the potentials, the five columns with the theoretical values in Table III are linearly dependent and the splittings resulting from our unperturbed wave functions for any choice of α_s, α_{2s}, and dV_1/dr can easily be reconstructed from the table.

V. CONCLUSIONS

Our analysis shows that it is possible to derive from first principles, at least within the quenched approximation, the spin-dependent potentials which determine the spin splittings within the heavy-quark families with an accuracy which permits meaningful quantitative comparisons between theory and experiment. The pattern of long- and short-range behavior of the various potentials is unambiguously fixed by the lattice calculation. The quenched approximation is seen to determine potentials which are too small in their short-distance component to account for the observed spin splittings, but, if one corrects for quark vacuum-polarization effects, one obtains results in good quantitative agreement with experiment, with the exception of the $1P$ states of the J/ψ family, where the predicted splittings are still too small. The correction for quark vacuum-polarization effects admittedly depends on adopting a definite prescription and does not follow directly from a simulation of the appropriate quantum fluctuations; still, like the rest of the computation and contrary to phenomenological approaches, it does not involve any adjustable parameter.

It would be clearly desirable to achieve a direct verification of the effects of quark vacuum polarization at short distances as well as a more accurate determination of the spin-dependent potentials at intermediate distances, one that could pinpoint any real deviation from the short-distance perturbative behavior. This would be only marginally possible with the computers available today, but will be certainly feasible with the new supercomputers, soon to be introduced. Then the parameters entering into the expansion of the Hamiltonian for large quark masses will be completely under control and it will be possible to evaluate the relevance of other effects, such as relativistic corrections or correction for neighboring open flavor channels, which, at some level, also affect the dynamics of heavy-quark bound states.

ACKNOWLEDGMENTS

We would like to thank Lloyd M. Thorndyke and Lee F. Kramer of ETA Systems, Inc., and Robert M. Price and Larry Jodsaas of Control Data Corporation for their continued interest, support, and access to the Cybernet CDC Cyber 205 at Rockville, Maryland, where all our computations have been made. We would also like to thank the Control Data Corporation PACER grants (Grants Nos. 85PCR06 and 86PCR01) for financial support and the Natural Sciences and Engineering Research Council of Canada (Grant No. NSERC A9030) for further financial support. This research was also carried out in part under the auspices of the U.S. Department of Energy under Contract No. DE-AC02-76CH00016.

[1]E. Eichten and F. Feinberg, Phys. Rev. Lett. **43**, 1205 (1979); Phys. Rev. D **23**, 2724 (1981).
[2]M. E. Peskin, in *Dynamics and Spectroscopy at High Energy,* proceedings of the 11th SLAC Summer Institute on Particle Physics, Stanford, California, 1983, edited by P. M. McDonough (SLAC Report No. 267, Stanford, 1984).
[3]D. Barkai, K. J. M. Moriarty, and C. Rebbi, Phys. Rev. D **30**, 1293 (1984).
[4]D. Barkai, K. J. M. Moriarty, and C. Rebbi, Phys. Rev. D **30**, 2201 (1984).
[5]S. Otto and J. D. Stack, Phys. Rev. Lett. **52**, 2328 (1984).
[6]N. A. Campbell, C. Michael, and P. Rakow, Phys. Lett. **139B**, 288 (1984).
[7]P. de Forcrand, in Proceedings of the Los Alamos Conference Frontiers of Quantum Monte Carlo, Los Alamos, New Mexico, 1985 [J. Stat. Phys. (to be published)].
[8]D. Gromes, Z. Phys. C **26**, 401 (1984).
[9]M. Campostrini, K. J. M. Moriarty, and C. Rebbi, Comput. Phys. Commun. **42**, 174 (1986).
[10]M. Campostrini, Phys. Lett. **147B**, 343 (1984).
[11]M. Campostrini, K. J. M. Moriarty, and C. Rebbi, Phys. Rev. Lett. **57**, 44 (1986).
[12]M. Campostrini, Nucl. Phys. **B256**, 717 (1985).
[13]C. Michael and P. E. L. Rakow, Nucl. Phys. **B256**, 640 (1985).
[14]P. de Forcrand and J. D. Stack, Phys. Rev. Lett. **55**, 1254 (1985).
[15]C. Michael, Phys. Rev. Lett. **56**, 1219 (1985); A. Huntley and C. Michael, Nucl. Phys. **B286**, 211 (1987).
[16]Y. J. Ng, J. Pantaleone, and S.-H. H. Tye, Phys. Rev. Lett. **55**, 916 (1985); J. Pantaleone, S.-H. Henry Tye, and Y. J. Ng, Phys. Rev. D **33**, 777 (1986).
[17]G. Parisi, R. Petronzio, and F. Rapuano, Phys. Lett. **128B**, 418 (1983).
[18]S. Gottlieb, P. B. Mackenzie, H. B. Thacker, and D. Weingarten, Nucl. Phys. **B263**, 704 (1986).
[19]D. Barkai, K. J. M. Moriarty, and C. Rebbi, Phys. Lett. **156B**, 385 (1985).